Chemistry–A European Journal
Research Article
doi.org/10.1002/chem.202401568
Chemistry Europe
European Chemical Societies Publishing
www.chemeurj.org

# Exohedral Diels-Alder Reactivity of Endohedral Metallofullerene $C_{36}$

Athul Santha Bhaskaran,[a] Dani Romero del Blanco,[a] Adrià Romero-Rivera,[a] Sílvia Osuna,*[a, b] and Marcel Swart*[a, b]

Understanding the exohedral reactivity of metallofullerenes is crucial for its application in various fields. By systematically controlling the trapped species inside the fullerene its reactivity can be tamed. In this work we report the preferential position of 3d metal atoms inside the $C_{36}$ cage and their effect on exohedral reactivity in comparison with the neutral and the dianionic cage. The Diels-Alder (DA) reaction between butadiene and all non-equivalent [5-5], [6-5] and [6-6] C–C bonds on the fullerene cage was considered for the analysis, by using density functional theory at the S12g/TZ2P level including COSMO solvation model to elucidate the complete mechanistic pathways. Our results indicate that the preferential position of the metal ion is at the position close to the upper hexagon, and that the general trend in the reactivity of bonds follows the order [5-5] > [6-5] > [6-6]. Moreover, the encapsulation of metal atoms further enhances the reactivity of these bonds, by lowering the LUMOs of the cage, hence maximizing the orbital interactions.

## Introduction

Fullerenes are a class of cage-like allotropes of carbon with an even number of carbon atoms ($C_{24}$, $C_{28}$, $C_{36}$, $C_{40}$, $C_{50}$, $C_{60}$, … $C_{2n}$). Since the discovery of the first fullerene $C_{60}$ in 1985,[1] it has been subjected to various theoretical and experimental studies which include encapsulating other molecules or metals inside the cage (endohedral fullerenes (EF) or endohedral metallofullerenes (EMF)) and doping the fullerenes with foreign atoms, among others.[2–4] The aforementioned methods can significantly influence the electronic and optical properties of fullerenes. EMFs are promising candidates with potential applications in the field of superconductivity, magnetism, and nonlinear optics.[5–6] The properties of EMFs can be tailored by varying the metal cluster inside the cage. Moreover, in principle we should be able to make EMFs lying at both ends of reactivity spectrum, inert and highly reactive. The relative inertness of the EMF carbon structure would make these compounds ideal for medical applications.[7–8] Furthermore, photon induced charge transfer using EMFs in electron donor-acceptor might lead to promising photovoltaic materials to be used in solar energy conversion/storage systems.[9] Finally, they can even serve as a probe in monitoring chemical reactions via changes in the electron paramagnetic resonance (EPR) signal.[10–11]

Several studies can be found in the literature that discuss the reactivity of EMFs.[4–14] Valladares *et al.* studied M@$C_{60}$ using conceptual density functional theory (DFT).[15] They found that if the metal atom stays at the center of the cage there is no significant difference in the reactivity compared to the pristine cage. However, when the preferred location of the metal is displaced from the center of the cage, like in the cases of Mn, Ni, Fe, and Co, the predicted reactivity changes drastically. Osuna *et al.* investigated the exohedral reactivity of $M_3N@C_{78}$,[16–17] and of $M_3N@C_{80}$,[18] amongst other encapsulated clusters. Most of these studies have been devoted to higher order fullerenes ($C_{2n}$, $2n > 50$). To the best of our knowledge, relatively few studies have been done on the reactivity of smaller fullerenes ($C_{20}$, $C_{28}$, $C_{36}$, ….). A recent study shows that $C_{36}$ and $C_{35}N$ are promising candidates to use as drug delivery nano vehicles for medical applications.[19] Moreover, endohedral mono-metallofullerenes of these smaller hollow cages ($C_{28}$, $C_{36}$, $C_{44}$ …) have been experimentally synthesized using bottom-up approach through $C_2$ insertion reaction.[20] The authors discuss how the metal-to-cage charge transfer is the driving process for the formation of large EMFs from smaller ones. This brings out more clarity on the distribution of charges on the small EMFs.

Our fullerene of interest $C_{36}$ was synthesized in the laboratory in 1998 by Zettl and co-workers, using the arc discharge method.[21] Unlike other higher order fullerenes, the anatomy of $C_{36}$ makes its more reactive.[22] Generally, the architecture of fullerenes contains hexagons and pentagons, where the number of pentagons and the empirical isolated pentagon rule (IPR).[23] dictate the stability of different isomers of fullerenes. Smaller fullerenes such as $C_{36}$ and several EFs are the exception to this empirical IPR rule. The structure of $D_{6h}$-$C_{36}$ consists of four different types of bonds (see Figure 2) namely [5-5] (type-E, pentalene), [6-5] (type-G and type-F), and [6-6] (type-A, pyracylene). Adjacent pentagon pairs (APPs) induce

[a] A. Santha Bhaskaran, D. Romero del Blanco, A. Romero-Rivera, S. Osuna, M. Swart
Institut de Química Computacional i Catàlisi and Departament de Química, Universitat de Girona, Parc R + i Univ. Girona, Ed. Monturiol, c/Emili Grahit 91, 17003 Girona, Spain
E-mail: silvia.osuna@icrea.cat
marcel.swart@icrea.cat
[b] S. Osuna, M. Swart
ICREA, Pg. Lluís Companys 23, 08010 Barcelona, Spain

Supporting information for this article is available on the WWW under https://doi.org/10.1002/chem.202401568

more strain in the molecular structure and thereby make it more reactive. $C_{36}$ and its derivatives are believed to make a class of promising materials with new structural and electronic properties, such as covalent bonding, high reactivity, significant steric strain, low band gap, high strength, and superconductivity.[24–25]

Fullerenes are involved in typical electron-deficient polyolefins reactions, such as reduction, cycloadditions, nucleophilic additions, hydrogenations, radical additions, halogenations. They can also form transition metal complexes and participate in hydrometallation reactions. They can be oxidized and give reactions with electrophiles.[26] Furthermore, fullerenes can participate in cycloaddition reactions like Diels-Alder (DA) with dienes; as a result, there are numerous computational and experimental studies focused on the DA cycloaddition on fullerene.[27] Several of these studies analyzed the effect of addition of *s-cis*-1,3-butadiene on the different C–C bonds of each carbon cage. In the case of $Sc_3N@C_{78}$, all endohedral species are less reactive than their homologous hollow cages.[17–28] When the $Sc_3N$ is encapsulated inside the icosahedral cage $I_h$-$C_{80}$, the [6-5] adduct is more stable than the [6-6] one by more than 12 kcal mol$^{-1}$. Another study was with $Ti_2C_2@D_{3h}$-$C_{78}$.[29] whose results showed that the regioselectivity of this exohedral addition is modified by changing the nature of the cluster encapsulated inside.

The preference for reacting with a given bond is due to different factors: first, (formal) charge transfer from the metallic cluster to the fullerene that changes the C–C bonds lengths (and thus their aromaticity).[30–32] Second, cage deformation/distortion caused by the metallic cluster, which has an important influence on the C–C bond lengths and their reactivity. This played a major role in the $Y_3N@C_{78}$ case,[16] where the metallic cluster does not fit so well inside; as result, the most reactive bond was a long C–C bond (normally the least reactive), found close to one the yttrium atoms. The cycloaddition of butadiene causes the cage to open around that bond, thus providing relief for the strain imposed by the yttrium, and hence, provided the most reactive bond. Third, stabilizing orbital interactions, i.e. better overlap between HOMO of diene and LUMO of cage at the transition state, leads to kinetic control [6-6] of product in the case of $C_{78}$ cage. As mentioned earlier, the $C_{78}$ is more reactive than $Sc_3N@C_{78}$ which is due to the less stabilizing orbital interactions between the EMF and the diene than $C_{78}$ and diene. This implies that $C_{78}$ makes a better dienophile than $Sc_3N@C_{78}$, leading to strong orbital interactions.[28] Furthermore, in general, the reactivity decreases when going from free $D_{3h}$-$C_{78}$ to $Ti_2C_2@D_{3h}$-$C_{78}$. $Ti_2C_2$ and $Sc_3N$ cluster have similar encapsulation energies and similar changes in reactivity, the most favored bond being [5-6] bonds close to the metals and [6-6] bonds far from the cluster,[31] in contrast to the encapsulation of $Y_3N$ inside the same isomer where the type-B [6-6] bond and the type-D [5-6] bond are the most favored. Moreover, encapsulation of $Y_3N$ and $Sc_3N$ inside the non-IPR $C_2$-$C_{78}$ cage has shown that type-E [5-5] bonds are by far the most reactive sites for the cycloaddition reaction. Therefore, it seems quite clear that the key factor that contributes to the exohedral reactivity of the $C_2$ isomer is the fullerene strain energy (at the pentalene units with the [5-5] bond) and not the nature of the encapsulated cluster. However, as mentioned before most of these studies are limited to the higher fullerenes.

In this work, we first investigate the preferential position of metal ions inside the clathrin analog of $C_{36}$ fullerene cage. We are also interested in exploring the exohedral reactivity of the endohedral metal doped $C_{36}$, as well as its pristine form to shed light on the reaction mechanism and the nature of chemical bonding.

## Results and Discussion

### Methodology

All the molecular structures of butadiene, fullerenes, EMFs, transition states (TS) and products are obtained with a dispersion corrected S12g-D3[33–34] functional and triple-zeta TZ2P basis set using the QUILD[35] optimizer within the Amsterdam Density Functional (ADF version 2019) program.[36] Subsequently, a frequency analysis is performed on the optimized geometries to make sure that they have no imaginary frequencies, i.e., that they are true minima. Transition states are characterized by one (and only one) imaginary frequency and all the intermediates are characterized by no imaginary frequency. We have carried out the optimization in acetonitrile solvent with a dielectric constant of 37.5. Solvent and scalar relativistic effects were considered in the optimization explicitly using the COSMO solvation model[37–38] and the ZORA Hamiltonian.[39]

### Endohedral Doped $C_{36}$

We aimed to study the preferential position of the 3d metal inside the endohedral doped fullerene $D_{6h}$-$C_{36}$. 3d metals such as Sc, Fe and Zn were considered at six non-equivalent positions inside the cage for the study. Metal atom could be located: (I) at the center of fullerene; or towards (II) the face of side hexagon; (III) the face of top hexagon; (IV) the face of pentagon; (V) [6-6] bond; (VI) [6-5] bond (see Figure 1).

Only one stable conformation was found for $[Zn^{2+}@C_{36}]^0$, which was at the center of the fullerene cage; this can be

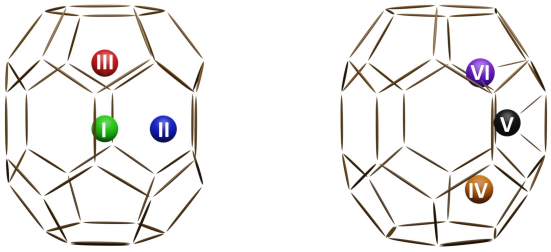


**Figure 1.** Different possible positional isomers of $M@C_{36}$ (M=Sc, Zn, and Fe). Metal atom located: (I) at the center; or towards (II) the face of side hexagon; (III) the face of top hexagon; (IV) the face of pentagon; (V) [6-6] bond; (VI) [6-5] bond.

understood as resulting from the size of Zn[40–41] (see Table 1) but also from the coordination chemistry preferences of Zn (see Supporting Information). The introduction of Zn causes an overall reduction in symmetry of the structure from $D_{6h}$ to $C_s$ due to the deformation of the cage (with a minimum Zn–C distance of 2.58 Å). The deformation of the cage compared to the neutral cage has been determined to be 11.2 kcal mol$^{-1}$. Three stable conformations were found for the $[Sc^{3+}@C_{36}]^+$ ($S=0$). The orientation of Sc towards the top hexagonal face corresponds to the minimum in energy structure. This preference to coordinate to hexagons is not like normal coordination chemistry trends: in complexes when it is free to move both Sc and Fe prefer to bind to pentagon rings (see SI). Introduction of Sc at location III causes a cage deformation of 7.1 kcal mol$^{-1}$ (see Table 2). In this binding mode Sc atom is coordinating to the pentagonal rings of $C_{36}$ fullerene cage with bond lengths of 2.26 Å, 2.41 Å, and 2.48 Å. Apparently, this enables the (formal) charge transfer between the metal and the fullerene that stabilizes the whole compound. Praseodymium and uranium are known examples that form EMFs Pr@$C_{82}$ and U@$C_{28}$.[42] These molecules are better described as $Pr^{3+}@C_{82}^{3-}$ and $U^{4+}@C_{28}^{4-}$ by using an ionic model.[42] The ionic model which describes the (formal) metal to cage charge transfer is consistent with the endohedral mono-metallofullerenes of group 4 metals (M@$C_{28}$) where the central metal atom exhibits a +4 oxidation state ($M^{4+}$).[43] Hence, the charge transfer and the oxidation state of the metal are the determining factors that govern the EMF formation.[20] In addition, higher order EMFs also exhibit the formal metal to cage charge transfer. In $M^{3+}@C_{n\geq 82}^{3-}$ (M=La, Y), X-ray photo emission spectroscopy data shows that the encapsulated La atom is in a formal oxidation close to the +3 state.[44] This study bring us to the conclusion that the metal to carbon bond has partial ionic character.

A high relative energy (30 kcal mol$^{-1}$) is observed when Sc is located at the center of the cage (see Table 1). For iron, we explored the different spin states and found that the lower $S=$

**Table 1.** Computed relative electronic energies in kcal mol$^{-1}$ of different possible conformers of endohedrally doped fullerene $C_{36}$.

| Metal | I | II | III | IV | V | VI |
|---|---|---|---|---|---|---|
| $[Sc@C_{36}]^+$ $S=0$ | 29.99 | 17.40 | 0.00 | | | |
| $[Zn@C_{36}]^0$ $S=0$ | 0.00 | | | | | |
| $[Fe@C_{36}]^0$ $S=0$ | 82.77[a]<br>45.71[b] | 26.40 | 0.00 | 13.59 | 23.19 | 11.10 |
| $[Fe@C_{36}]^0$ $S=1$ | 35.24 | 18.97 | 13.08 | 18.37 | 23.77 | 16.45 |
| $[Fe@C_{36}]^0$ $S=2$ | 32.36 | 21.25 | 25.23 | 26.50 | 17.78 | 19.20 |

[a] Closed shell singlet; [b] Open-shell quintet coupled anti-ferromagnetically to quintet state on the fullerene.

**Table 2.** Computed barrier heights for first TS ($\Delta G^{\neq}$) and reaction energies ($\Delta G_r$) at 298 K in kcal mol$^{-1}$ of different types of bonds in both pristine and EMF $C_{36}$.

| System | 5-5 | | 6-5Gh | | 6-5Gp | |
|---|---|---|---|---|---|---|
| | $\Delta G^{\neq}$ | $\Delta G_r$ | $\Delta G^{\neq}$ | $\Delta G_r$ | $\Delta G^{\neq}$ | $\Delta G_r$ |
| $[C_{36}]$ $S=0$ | 10.5 | −38.8 | 12.6 | −36.7 | 11.4 | −37.6 |
| $[C_{36}]^{2-}$ $S=0$ | 15.8 | −32.0 | 18.5 | −27.0 | 18.5 | −27.7 |
| $[Sc@C_{36}]^+$ $S=0$ | 11.0 | −38.8 | 9.1 | −32.2 | 8.5 | −33.0 |
| $[Zn@C_{36}]^0$ $S=0$ | 17.0 | −41.8 | 14.1 | −34.5 | 13.2 | −35.4 |
| $[Fe@C_{36}]^0$ $S=0$ | 13.2 | −43.1 | 13.2 | −41.1 | 13.1 | −23.7 (−41.9) |
| $[Fe@C_{36}]^0$ $S=1$ | 29.2 | −35.9 | 27.8 | −29.1 | 27.3 | −30.0 |
| $[Fe@C_{36}]^0$ $S=2$ | 25.2 | −26.1 | 28.7 | −18.3 | 27.9 | −19.5 |
| System | 6-5Fh | | 6-5Fp | | 6-6 | |
| | $\Delta G^{\neq}$ | $\Delta G_r$ | $\Delta G^{\neq}$ | $\Delta G_r$ | $\Delta G^{\neq}$ | $\Delta G_r$ |
| $[C_{36}]$ $S=0$ | 9.2 | −28.2 | 8.2 | −29.0 | 21.7 | 2.8[a]–14.3[b] |
| $[C_{36}]^{2-}$ $S=0$ | 14.7 | −22.8 | 14.6 | −23.5 | 28.0[c] | 3.8[a]–11.3[b] |
| $[Sc@C_{36}]^+$ $S=0$ | 11.0 | −32.1 | 10.4 | −32.9 | 13.1[c] | −15.0[a]–38.4[b] |
| $[Zn@C_{36}]^0$ $S=0$ | 10.2 | −36.9 | 9.7 | −37.7 | 19.1[c] | −9.9[a]–28.3[b] |
| $[Fe@C_{36}]^0$ $S=0$ | 13.7 | −26.9 | 13.1 | −27.8 | 21.0[c] | −5.3[a]–19.9[b] |
| $[Fe@C_{36}]^0$ $S=1$ | 25.0 | −21.3 | 24.8 | −22.2 | 32.3 | −0.2[a]–14.6[b] |
| $[Fe@C_{36}]^0$ $S=2$ | 24.4 | −19.5 | 24.7 | −19.9 | 32.5 | 2.7[a]–16.9[b] |

[a] [4+2] product. [b] [4+3] product. [c] [4+3] TS, values in the parenthesis correspond to the thermodynamic product. $\Delta G^{\neq}$ = G(TS)−(G(M@$C_{36}$/$C_{36}$/$C_{36}^{2-}$)+G(diene)), $\Delta G_r$ = G([4+2] product/[4+3] product)−(G(M@$C_{36}$/$C_{36}$/$C_{36}^{2-}$)+G(cis-diene)).

**Table 3.** Computed C–C bond lengths (in Å) of different bonds in pristine and endohedrally doped fullerene $C_{36}$.

| Bond | $C_{36}$ (Å) | $C_{36}^{2-}$(Å) | $[Sc@C_{36}]^{+}$ $S=0$ (Å) (min-max) | $[Zn@C_{36}]^{0}$ $S=0$ (Å) (min–max) | $[Fe@C_{36}]^{0}$ $S=0$ (Å) (min–max) |
|---|---|---|---|---|---|
| Type-A (6-6) | 1.433 | 1.437 | 1.439–1.439 | 1.447–1.447 | 1.418–1.418 |
| Type-G (6-5) | 1.407 | 1.414 | 1.413–1.432 | 1.415–1.415 | 1.423–1.475 |
| Type-F (6-5) | 1.425 | 1.432 | 1.431–1.441 | 1.433–1.439 | 1.442–1.446 |
| Type-E (5-5) | 1.480 | 1.471 | 1.469–1.471 | 1.464–1.489 | 1.443–1.466 |

0 spin state is preferred over the higher ones, as one would expect for a $d^6$ system. All six possible conformers were stable structures for $[Fe^{2+}@C_{36}]^{0}$ ($S=0$), although with considerable differences in stability (see Table 1). Like the Sc case, the conformer in which Fe is close to the hexagonal face surrounded by the pentagonal architecture is the most stable conformer, which is consistent with theoretical calculations by Estrada *et al.* on the $Fe@C_{60}$ fullerene.[15] Among all other metals, iron is closer to the carbon atom (the smallest Fe–C distance is 1.89 Å) of the cage thereby causing more structural distortion to the cage (see Table 3). For singlet and triplet, the orientation III was the most stable one, whereas for quintet the orientation V, with Fe being located towards the [6-6] bond, is the preferred position. The singlet-triplet energy gap was found to be 13.1 kcal mol$^{-1}$.

Interestingly, the $[Fe^{2+}@C_{36}]^{0}$ system changes spin state depending on the position of the metal inside the cage. For all positions except at the center, the iron is found in a closed-shell singlet state; however, at the center it switches over to an open-shell quintet, coupled anti-ferromagnetically to a quintet electronic structure. This spin-state switching lowers the relative energy by ca. 46 kcal mol$^{-1}$, still it is very unstable compared to the other locations (see Table 1).

## Exohedral Reactivity of $C_{36}$ Fullerenes

After the study of the preferred location (and in some cases spin state) for the different metals, we have analyzed the exohedral reactivity of the most stable conformers of endohedral metallofullerenes and compared them to the pristine case. DA reactions between s-*cis*-1,3-butadiene, and all non-equivalent C–C bonds of $C_{36}$ and $M@C_{36}$ were considered for the analysis. We have four non-equivalent bonds in the cage: (I) type-E [5-5] bond; (II) type-F [6-5] bond; (III) type-G [6-5] bond; (IV) type-A [6-6] bond. In addition, for type-F and type-G bonds two possible DA adducts can be obtained (see Figure 2): the attack by butadiene can take place with the diene oriented towards the hexagonal side (6-5Gh) or towards the pentagonal side (6-5Gp).

## Exohedral Reactivity of Empty $C_{36}$

In the case of pristine $C_{36}$ and $C_{36}^{2-}$, when examining the geometries of the species in both instances, type-E [5-5] bond

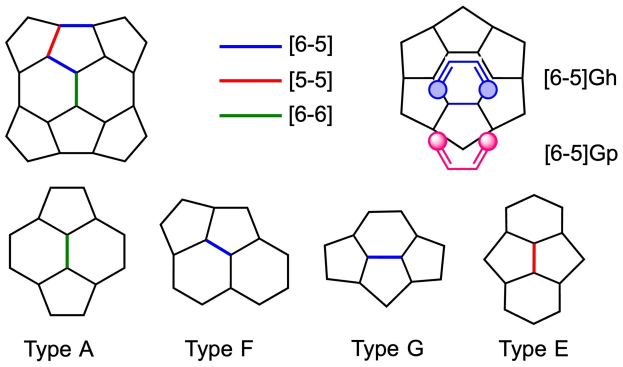


**Figure 2.** Type of bonds in $C_{36}$. [6-6] bond (type A), [6-5] bonds (type F and type G) and [5-5] bond (type E). The DA reaction on type-G bonds can take place with the diene oriented towards the hexagonal side (6-5Gh) or towards the pentagonal side (6-5Gp).

was identified as the longest, and type-G [6-5] bond being the shortest (see Table 3). Furthermore, addition of two electrons to the neutral cage causes a deformation of 6 kcal/mol of the dianionic cage. Upon reviewing the thermodynamic stability of products and TSs in both cases, the longest [5-5] bond was found to be the most reactive, whereas the [6-6] bond is the least reactive one (see Table 2); among the [6-5] bonds, type-G was more reactive than type-F. With the dianionic cage, the [6-6] bond, despite being least reactive, shows an unprecedented [4+3] addition reaction instead of the normal [4+2] DA cycloaddition. All [6-5] bonds, except the $C_{36}$ type-G followed the one-step polar asynchronous TS, whereas $C_{36}$ type-G bond followed non-polar synchronous TS. Notably, both the $C_{36}$[6-6] and $C_{36}^{2-}$[5-5] bonds followed two step reaction mechanisms involving two TSs. There was a small difference (less than 1 kcal mol$^{-1}$) in the stability of products and TS in the case of different conformers possible for the [6-5] bonds species. The attack from the pentagon side is slightly favored over the attack from the hexagon side.

Overall, the neutral cage is more reactive than the dianionic cage. This can be understood by looking at the frontier MOs: for $C_{36}$ the dienophile LUMO is closer to the HOMO of diene, favoring the normal demand DA reaction. Instead, the extra two electrons on the $C_{36}^{2-}$ cage raise the energy of its filled orbital in such a way that the interaction between the HOMO of dienophile and LUMO of diene becomes the most stabilizing interaction, thereby favoring the inverse-electron-demand Diels-Alder reaction (iEDDA).

To gain additional insights of the chemical bonding patterns, we have explored the importance of the different

energy components with the activation strain model (ASM)[45–46] of the TS (see Figure 4). According to the model, the activation energy at the transition state can be decomposed into interaction energy and strain energy given by the equation ($\Delta E^{\neq} = \Delta E^{\neq}_{int} + \Delta E^{\neq}_{strain}$).

In some cases, this leads to a negative activation energy, which is shown e.g. with the overall barrier of bimolecular substitution ($S_N2$) reactions. In the gas phase with anionic nucleophiles it is often observed[47] that this overall barrier is negative, even though the central barrier is (of course) positive and substantial. Here, bringing the diene and dienophile fragment together leads to a similar situation, where there exists a sizeable central barrier (as shown in Figure S4), but the TS is stabilized compared to the reactants infinitely separated from each other. As a result, for the $C_{36}$ cage the interaction energy wins over the deformation energy whereas it is vice versa in the case of $C_{36}^{2-}$. It indicates that the major driving force for the reaction in the case of $C_{36}$ is the interaction energy, whereas for $C_{36}^{2-}$ it is the strain energy.

The interaction energy can be further decomposed into five terms namely, electrostatic interaction, Pauli repulsion (or exchange repulsion), (attractive) orbital interactions, dispersion energy and solvent reorganization energy[48] (Equation 1)

$$\Delta E_{int} = \Delta E_{pauli} + \Delta E_{elstat} + \Delta E_{orbit} + \Delta E_{disp} + \Delta E_{solv} \quad (1)$$

Here, $\Delta E_{Pauli}$ comprises destabilizing steric repulsion between occupied orbitals; $\Delta E_{elstat}$ corresponds to the classical electrostatic interaction between the fragments; $\Delta E_{orbit}$ the orbital contribution term involves the orbital interaction between the interacting fragments, which include HOMO-LUMO interactions. The other two terms are the dispersion energy ($\Delta E_{disp}$) and solvent reorganization energy components ($\Delta E_{solv}$) of the interactions.

In the case of pristine cages when comparing the energy decomposition analysis (EDA) contributions at the TS (Figure S4), it becomes clear that there is a significant difference in the Pauli repulsion term for different bonds involved in the reaction. Pauli repulsion is ca. 125 kcal mol$^{-1}$ larger, or more, for the [6-6] bond compared to other bonds. This in turn closely correlates with the higher activation barrier for [6-6] bond, which we tried (unsuccessfully) to trace back to the change of the overlap of the frontier MOs (see SI Table S8). However, the energy decomposition along the reaction coordinates reveals that the origin of the difference in the reactivity of [5-5] and [6-6] bonds come from the difference in orbital interactions (see Figure 4). A similar conclusion can be derived when comparing the reactivities of 6–5 bonds, where type-F is more stable than type-G due to the orbital interaction stabilizing factor. Similar types of observations have been reported in the literature for $C_{60}$ fullerene, where the selectivity of the [6-6] bond over the [6-5] bond was based on the difference in the orbital interactions of the diene and the cage.[49–50] The electrostatic interaction and orbital interactions are also correlating with the activation energy barrier and stability of the products. On the other hand, $\Delta E_{disp}$ and $\Delta E_{solv}$ are almost constant for every bond (see Table S2 Supporting Information).

## Exohedral Reactivity of Endohedrally Doped $C_{36}$

The study of the reactivity of $[Sc@C_{36}]^+$ indicates that it follows a similar trend to that of the pristine ones (see Table 2), where the reactivity of type-G and type-F bonds are almost equivalent. Similarly to the pristine cage, an unprecedented [4+3] addition was observed in the case of the [6-6] bond. Notably, the [5-5] bond follows a one-step polar asynchronous TS. Upon examining the activation strain relationship of the components, it is evident that the interaction energy is always higher than the deformation/preparation energy. In combination with the HOMO-LUMO diagram (see Figure 3) we can conclude that all bonds in $[Sc@C_{36}]^+$ follow a normal demand DA reaction.

The HOMO-LUMO levels of $[Zn@C_{36}]^0$ are matching with the neutral cage so one would expect similar type reactivity patterns as those of the neutral cage. Although the reactivity of different bonds in $[Zn@C_{36}]^0$ is like the $[Sc@C_{36}]^+$ case, the reaction pathways are different. Both [5-5] bond and the type-G [6-5] bond follow a one-step polar asynchronous TS, whereas the two-step reaction pathway is observed in the case of type-F [6-5] bond. Unlike other cases, in $[Zn@C_{36}]^0$ the type-F [6-5] bond is more reactive than the type-G. With Zn we also observed the [4+3] adduct, which is more stable than the DA adduct. All these observations are explained by the activation strain profile at the TS of different types of bonds and by comparing the lobe size of low lying LUMOs. All together there is a favorable type of (secondary orbital) (see Table S4) interactions present in the case of type-F [6-5] bond that leads to the stabilization of transition state. The close in energy LUMO with respect to the HOMO of diene results in the possibility of normal demand DA reaction in the case of zinc doped fullerene.

Irrespective of the spin state, the [5-5] bond is the most reactive bond in $[Fe@C_{36}]^0$ followed by [6-5] bonds, and finally the [6-6] bond. In the case of [6-5] bonds, all the bonds close to the iron atom exhibit equal energy transition states and there was no significant difference if the diene is pointing to the hexagonal face or pentagonal face, which is likely due to the metal pushing the orbitals of the fullerene outwards. Despite the reactivity, type-G followed two step mechanism and type-F proceeded via one step polar asynchronous pathway. On top of that, the [6-6] bond preferred [4+3] product over DA product.

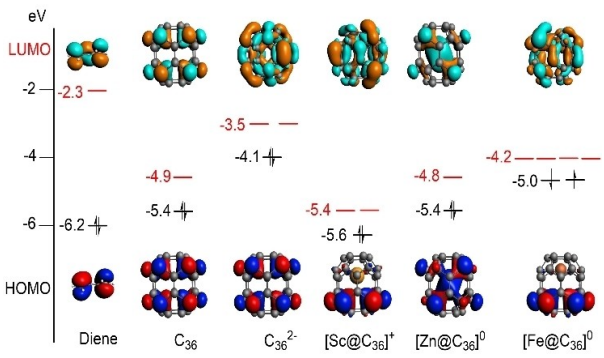


**Figure 3.** HOMO-LUMO diagrams of stable isomers of EMFs, diene, and pristine cages. All the values are in eV (isosurface value = 0.03).

A detailed analysis of the overall reaction pathway unveiled that the [5-5] bond follows a two-step mechanism in all the higher spin states. For instance, in the quintet state all bonds followed the two-step mechanism whereas at the singlet state only type-G proceeds via two-step mechanism; all other bonds follow the one-step mechanism. The TS for the DA product at singlet state was not observed for the [6-6] bond (see Table S3), conversely higher spin states favored the two-step DA process, and all the TSs were identified. There is no significant difference ($\Delta\Delta G^{\neq}_{q-t} < 1$ kcal mol$^{-1}$) in the Gibbs free energies of triplet and quintet species at the TS except for the [5-5] bond ($\Delta\Delta G^{\neq}_{q-t} =$ 4.0 kcal mol$^{-1}$) with preference for the quintet.

The movement of the Fe atom inside the cage, away from the reaction site, was observed for all bonds. For instance, when studying the type-G bond, a significant repositioning of Fe atom from position (III) to position (IV) was observed. This repositioning provides an extra stability to the final product because of the favorable Fe-pentagon interaction and the lower cage deformation energy of the final geometry (see Table 2).

In the case of open shell systems, activation energy at the TS can be decomposed into interaction energy and preparation energy, given by the equation ($\Delta E^{\neq} = \Delta E^{\neq}_{int} + \Delta E^{\neq}_{prep}$).[51] Preparation energy can be further decomposed into strain/deformation energy and valence excitation energy; the latter term considers the spin flipping contribution during the course of the reaction. I.e., when performing the ASM analysis for the triplet or quintet state, we need to consider the metallocage separately, in which case the $S=0$ state is lowest in energy. For the ASM of course we consider the interaction of the diene with the metallocage in the $S=1$ (triplet) or $S=2$ (quintet) state. This change in spin state (of the metallocage alone) costs energy, which is called the valence excitation energy. Therefore, for singlet case the energies are the same ($\Delta E^{\neq}_{prep} = \Delta E^{\neq}_{strain}$), while for triplet/quintet the valence excitation energy needs to be added. In conclusion, for Fe $S=1$ all the bonds close to the metal except the [6-6] bond is equally reactive under kinetic control but the cycloadduct of type E [5-5] is the desired product under thermodynamic control. When the bonds are distant from the metal atom, we observed a rise in the barrier height and free energy of the reaction; these result in less favorable DA reaction at those bonds (see Table S3). Whereas, for Sc the trend is opposite to that of Fe where the desired product is the one in which the metal is away from the bond.

For fullerenes, the thermodynamic stability of the products is linked with their pyramidalization angles ($\theta_p$)[52] of the bonds. A higher value of the pyramidalization angle implies the system is highly strained. To release this strain, the bond will undergo cycloaddition reactions by making a thermodynamically stable product. In our fullerenes the most strained bond in terms of $\theta_p$ is the type E pentalene bond which in turn indicates that the cycloadduct of this bond is the most stable among others. In fact, this observation would make more sense when explaining the relative inertness of type A [6-6] bond, which is the bond having the smallest pyramidalization angle. Pyramidalization angles alone are not sufficient to explain the complete reactivity patterns of the fullerenes. In that case, HOMO-LUMO diagrams give more qualitative picture of the story. The kinetics of the reaction is more dependent on the orbital interactions as derived from the ASM and EDA analysis. We can also draw conclusions from the LUMOs of the fullerenes. The LUMOs diagrams qualitatively correlated with the barrier heights of the reaction. Also, one could argue that the low lying LUMO+2 orbitals favor the exothermic formation of [4+2] cycloadducts in the case of [6-6] bonds of EMFs compared to the pristine fullerenes.

Similarly, as observed for pristine $C_{36}^{0/2-}$, when applying the ASM model to the iron systems in the singlet ground state, most bonds show an overall barrier which is close to zero; except for [6-6] bond with substantial overall barrier. The higher spin states have high barriers due to the contribution from the spin flipping part in the valence excitation energy. When we compare the triplet and quintet states similar reactivity trends are found. The HOMO-LUMO analysis indicates that the 4 close-lying LUMOs of $[Fe@C_{36}]^0$ are closer to the HOMO of the diene, which results in a better overlap and favors the normal demand DA reaction.

### ASM and EDA Along the Reaction Coordinate

The application of the ASM model focuses on bringing together two fragments, which might not always provide meaningful insights into the origin of the chemical barrier.[45–53] Therefore, Bickelhaupt and co-workers have often followed the ASM energies along the Potential Energy Surface (PES), to be able to investigate what causes the barrier, and how this is changed by substituent effects, solvation, etc. Here, we have explored the PES through constrained optimizations where the incoming shortest C(cage)-C(diene) bond is varied in steps of 0.1 Å, from 3.55 Å to shortest TS distance. For each of these C–C distances a full optimization is carried out, while keeping this C–C distance fixed through a constraint.[54] Afterwards, for each of these points we have carried out the usual ASM analysis. We have done this PES scan of the ASM only for the most reactive bonds, and for Fe only considering the $S=0$ ground state. Upon examining the ASM profiles, unlike the pristine cages the [6-6] bonds of EMFs are more reactive (activation energy is close to zero or negative) except for iron where the bond shortening was observed. The EDA along the reaction coordinate unveils that the orbital interaction and Pauli term is more predominant in [6-6] bond than [5-5], this can also be inferred from the HOMO-LUMO picture of the reacting species. Therefore, the explanation for the higher barrier for [6-6] bonds come from the Pauli component of the interaction and strain energy of the overall systems (see Figure 4). Moreover, the regio selectivity of [6-5] bonds can be deciphered by the same reasoning (Figure S3).

## Conclusions

The most stable position of the 3d metal inside the barrel shaped $C_{36}$ cage was studied computationally using DFT. Also, the exohedral reactivity of the most stable conformer of the

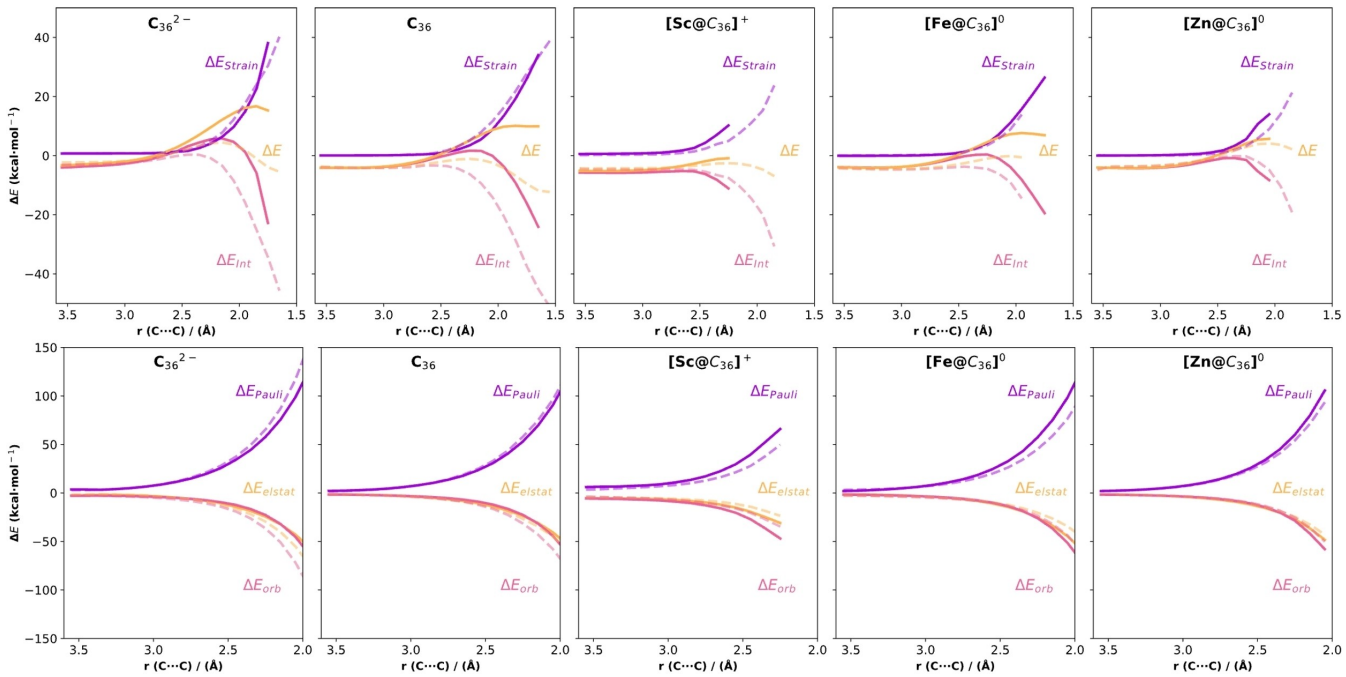


**Figure 4.** Activation strain analysis (ASM) along the reaction coordinates of [6-6] (solid line) and [5-5] (dotted line) bonds. Diels-Alder reactions between cage (cage = $C_{36}$ and $C_{36}^{2-}$) and *s-cis*-1,3-butadiene are studied. All energies are expressed in kcal mol$^{-1}$.

fullerene cage was explored by studying the DA reaction between the cage and s-*cis*-1,3-butadiene. Our calculations reveal that depending on the 3d metal the orientation inside the cage is different. For instance, Sc, Fe-singlet and Fe-triplet preferred the orientation towards the top hexagonal face of the barrel like cage (III). On the other hand, Zn prefers the center of the fullerene cage and Fe quintet coordination the [6-6] bond. A significant amount of spin splitting energy was found in the case of singlet, triplet, and quintet states of Fe, with $S = 0$ as the ground state. Based on the relative energies of DA products and large $\theta_p$ value we can conclude that the [5-5] bond is the most reactive bond in both the pristine $C_{36}$ and EMF $C_{36}$. This regioselectivity towards the [5-5] bond can be explained by the extra stabilization of transition states by interaction energy through orbital interactions in the case of pristine cages and combined effect of strain and orbital interactions in the case of EMFs. The addition of extra two electrons make the $C_{36}$ cage less reactive compared to the neutral one. The frontier MO (HOMO(diene)-LUMO(fullerene)) energy levels reveal that almost all fullerenes follow normal demand DA reaction; being the only exception the dianionic cage which follows the inverse electron demand pathway.

However, the reaction pathway can be tailored by changing the endohedrally doped species. The reactivity of various bonds of the $C_{36}$ cage follows the order [5-5] > [6-5] > [6-6]. Among the [6-5] bonds, except for the zinc case, type-G is more reactive than type-F due to the bond strain and percentage of the LUMO lobes on the bond determined by the positioning of the bond in the molecular cage structure. Altogether our computational investigation on the small $C_{36}$ and metal doped $C_{36}$ fullerene cages indicates that in terms of the thermodynamic control type-G is more reactive than type-F. Overall both the $C_{36}^{0/2-}$ and the EMFs are very reactive in nature (mostly the activation energies are negative or close to zero). However, the low lying LUMOs present in the EMFs compared to the pristine fullerenes make them favorable candidate for the cycloaddition reaction. This in turns explains the regioselectivity of these DA reactions.

## Supporting Information Summary

The authors have cited additional references within the Supporting Information.

## *Acknowledgements*

We thank the EU (ERC-2022-CoG-101088032 to S.O.), AEI/MCIU (PID2020-114548GB-I00 to M.S., PID2021-129034NB-100 to S.O.), GenCat (2015_FI_B_00165 fellowship to A.R-R., grant 2021SGR00487 to S.O.), Univ. Girona (IFUdG 68 2022 fellowship to A.S.B.) and a developer's license to M.S. by SCM for financial support. Open Access funding provided thanks to the CRUE-CSIC agreement with Wiley. Prof. M. Solà is thanked for discussions at the initial stages of this project.

## *Conflict of Interests*

The authors declare no conflict of interest.

## Data Availability Statement

Open data is available on iochem-bd using the following link for DOI 10.19061/iochem-bd-4-72: http://doi.org/10.19061/iochem-bd-4-72.

**Keywords:** Fullerene · Density functional theory · Diels-Alder reaction · 3d metals · Reactivity

[1] H. W. Kroto, J. R. Heath, S. C. O'Brien, R. F. Curl, R. E. Smalley, *Nature* **1985**, *318*, 162–163.
[2] A. A. Popov, S, Yang, L. Dunsch, *Chem. Rev.* **2013**, *113*, 5989–6113.
[3] J. M. Campanera, C. Bo, M. M. Olmstead, A. L. Balch, J. M. Poblet, *J. Phys. Chem. A* **2002**, *106*, 12356–12364.
[4] S. Osuna, M. Swart, M. Solà, *Phys. Chem. Chem. Phys.* **2011**, *13*, 3585–3603.
[5] H. Hu, W.-D. Cheng, S.-P. Huang, Z. Xie, H. Zhang, *J. Theor. Comput. Chem.* **2008**, *07*, 737–749.
[6] D. B. Whitehouse, A. D. Buckingham, *Chem. Phys. Lett.* **1993**, *207*, 332–338.
[7] M. D. Shultz, J. C. Duchamp, J. D. Wilson, C.-Y. Shu, J. Ge, J. Zhang, H. W. Gibson, H. L. Fillmore, J. I. Hirsch, H. C. Dorn, P. P. Fatouros, *J. Am. Chem. Soc.* **2010**, *132*, 4980–4981.
[8] M. D. Diener, J. M. Alford, S. J. Kennel, S. Mirzadeh, *J. Am. Chem. Soc.* **2007**, *129*, 5131–5138.
[9] D. M. Guldi, L. Feng, S. G. Radhakrishnan, H. Nikawa, M. Yamada, N. Mizorogi, T. Tsuchiya, T. Akasaka, S. Nagase, M. Ángeles Herranz, N. Martín, *J. Am. Chem. Soc.* **2010**, *132*, 9078–9086.
[10] G.-W. Wang, M. Saunders, R. J. Cross, *J. Am. Chem. Soc.* **2001**, *123*, 256–259.
[11] B. Pietzak, A. Weidinger, K.-P. Dinse, A. Hirsch, in *Endofullerenes New Fam. Carbon Clust.* (Eds: T. Akasaka, S. Nagase), Springer Netherlands, Dordrecht **2002**, 13–65.
[12] M. Pavanello, A. F. Jalbout, B. Trzaskowski, L. Adamowicz, *Chem. Phys. Lett.* **2007**, *442*, 339–343.
[13] W. Cai, M. Zhang, L. Echegoyen, X. Lu, *Fundam. Res.* **2023**, DOI: 10.1016/j.fmre.2023.12.004.
[14] J. Zhang, S. Stevenson, H. C. Dorn, *Acc. Chem. Res.* **2013**, *46*, 1548–1557.
[15] R. E. Estrada-Salas, A. A. Valladares, *J. Phys. Chem. A* **2009**, *113*, 10299–10305.
[16] S. Osuna, M. Swart, M. Solà, *J. Am. Chem. Soc.* **2009**, *131*, 129–139.
[17] S. Osuna, M. Swart, J. M. Campanera, J. M. Poblet, M. Solà, *J. Am. Chem. Soc.* **2008**, *130*, 6206–6214.
[18] S. Osuna, A. Rodríguez-Fortea, J. M. Poblet, M. Solà, M. Swart, *Chem. Commun.* **2012**, *48*, 2486–2488.
[19] M. Reina, C. A. Celaya, J. Muñiz, *ChemistrySelect* **2021**, *6*, 4844–4858.
[20] P. W. Dunk, M. Mulet-Gas, Y. Nakanishi, N. K. Kaiser, A. Rodríguez-Fortea, H. Shinohara, J. M. Poblet, A. G. Marshall, H. W. Kroto, *Nat. Commun.* **2014**, *5*, 5844.
[21] C. Piskoti, J. Yarger, A. Zettl, *Nature* **1998**, *393*, 771–774.
[22] P. W. Fowler, D. Mitchell, F. Zerbetto, *J. Am. Chem. Soc.* **1999**, *121*, 3218–3219.
[23] H. W. Kroto, *Nature* **1987**, *329*, 529–531.
[24] A. Koshio, M. Inakuma, T. Sugai, H. Shinohara, *J. Am. Chem. Soc.* **2000**, *122*, 398–399.
[25] A. Koshio, M. Inakuma, Z. W. Wang, T. Sugai, H. Shinohara, *J. Phys. Chem. B* **2000**, *104*, 7908–7913.
[26] W. E. Billups, *J. Am. Chem. Soc.* **2005**, *127*, 11876–11876.
[27] S. Osuna, M. Swart, M. Solà, *Phys. Chem. Chem. Phys.* **2011**, *13*, 3585–3603.
[28] F. M. Bickelhaupt, M. Solà, I. Fernández, *Chem. Eur. J.* **2015**, *21*, 5760–5768.
[29] S. Osuna, R. Valencia, A. Rodríguez-Fortea, M. Swart, M. Solà, J. M. Poblet, *Chem. Eur. J.* **2012**, *18*, 8944–8956.
[30] M. Garcia-Borràs, S. Osuna, J. M. Luis, M. Swart, M. Solà, *Chem. Soc. Rev.* **2014**, *43*, 5089–5105.
[31] M. Garcia-Borràs, S. Osuna, M. Swart, J. M. Luis, M. Solà, *Angew. Chem. Int. Ed.* **2013**, *52*, 9275–9278.
[32] M. Solà, *Nat. Chem.* **2022**, *14*, 585–590.
[33] S. Grimme, J. Antony, S. Ehrlich, H. Krieg, *J. Chem. Phys.* **2010**, *132*, 154104.
[34] M. Swart, *Chem. Phys. Lett.* **2013**, *580*, 166–171.
[35] M. Swart, F. M. Bickelhaupt, *J. Comput. Chem.* **2008**, *29*, 724–734.
[36] G. te Velde, F. M. Bickelhaupt, E. J. Baerends, C. Fonseca Guerra, S. J. A. van Gisbergen, J. G. Snijders, T. Ziegler, *J. Comput. Chem.* **2001**, *22*, 931–967.
[37] C. C. Pye, T. Ziegler, *Theor. Chem. Acc.* **1999**, *101*, 396–408.
[38] A. Klamt, G. Schüürmann, *J. Chem. Soc. Perkin Trans.* **1993**, *2*, 799–805.
[39] E. van Lenthe, E. J. Baerends, J. G. Snijders, *J. Chem. Phys.* **1993**, *99*, 4597–4610.
[40] S. Alvarez, *Dalton Trans.* **2013**, *42*, 8617–8636.
[41] B. Cordero, V. Gómez, A. E. Platero-Prats, M. Revés, J. Echeverría, E. Cremades, F. Barragán, S. Alvarez, *Dalton Trans.* **2008**, *2008*, 2832–2838.
[42] P. W. Dunk, N. K. Kaiser, M. Mulet-Gas, A. Rodríguez-Fortea, J. M. Poblet, H. Shinohara, C. L. Hendrickson, A. G. Marshall, H. W. Kroto, *J. Am. Chem. Soc.* **2012**, *134*, 9380–9389.
[43] A. Miralrio, L. E. Sansores, *Comput. Theor. Chem.* **2016**, *1083*, 53–63.
[44] J. H. Weaver, Y. Chai, G. H. Kroll, C. Jin, T. R. Ohno, R. E. Haufler, T. Guo, J. M. Alford, J. Conceicao, L. P. F. Chibante, A. Jain, G. Palmer, R. E. Smalley, *Chem. Phys. Lett.* **1992**, *190*, 460–464.
[45] I. Fernández, F. M. Bickelhaupt, *Chem. Soc. Rev.* **2014**, *43*, 4953–4967.
[46] F. M. Bickelhaupt, *J. Comput. Chem.* **1999**, *20*, 114–128.
[47] T. A. Hamlin, M. Swart, F. M. Bickelhaupt, *ChemPhysChem* **2018**, *19*, 1315–1330.
[48] K. Morokuma, *J. Chem. Phys.* **1971**, *55*, 1236–1244.
[49] I. Fernández, M. Solà, F. M. Bickelhaupt, *Chem. Eur. J.* **2013**, *19*, 7416–7422.
[50] I. Fernández, *Eur. J. Org. Chem.* **2018**, *2018*, 1394–1402.
[51] M. Swart, *Inorganica Chim. Acta* **2007**, *360*, 179–189.
[52] R. C. Haddon, *Science* **1993**, *261*, 1545–1550.
[53] Y. García-Rodeja, M. Solà, F. M. Bickelhaupt, I. Fernández, *Chem. Eur. J.* **2017**, *23*, 11030–11036.
[54] J. Baker, *J. Comput. Chem.* **1992**, *13*, 240–253.

Manuscript received: April 22, 2024
Accepted manuscript online: July 22, 2024
Version of record online: September 17, 2024